Proc. Fourth International Conference on Numerical Methods in Geomechanics, Edmonton, Canada, May 31-June 4, 1982, Vol. I, pp. 53-60.

A Circular Boundary Element for the Analysis of Deep Underground Openings.

I. D. MOORE,
Research Student, School of Civil & Mining Engineering, Univ. of Sydney, Sydney, Australia.

J. R. BOOKER
Reader in Civil Engineering, University of Sydney, Sydney, Australia.

SYNOPSIS In the study of underground openings it is necessary, in all but the simplest situations, to use an approximate numerical procedure, such as the finite element method. In conventional analyses it is usually necessary to utilise an extensive finite element mesh to adequately model the response of the surrounding material.

In this paper a circular boundary element which overcomes this difficulty is developed. The materia outside the circular boundary is approximated by an infinite number of annular regions with a constant ratio of interior to exterior radius. Each annulus is divided into a number of identical finite elements. The boundary stiffness of the complete body is then found analytically from the stiffness of these constitutent elements.

The adoption of this boundary element ensures accurate modelling of the behaviour of deep undergroun openings and permits substantial computational savings. Its use is illustrated by a variety of problems.

INTRODUCTION

It is often necessary to determine the distribution of stress in the neighbourhood of an underground opening. Analytic solutions have been found for certain, simple cases on the assumption that the surrounding material is an isotropic elastic solid. (Savin (1961), Muskhelishvili (1963) Obert and Duval (1967), Hoeg (1968)). However for more complicated situations involving complex geometries or material behaviour it is usually necessary to obtain solutions by using an approximate numerical technique such as the Finite Element Method, Zienkiewicz (1977).

In an conventional static finite element analysis it is not normally possible to take into account infinitely distant boundaries although this is often done for the dynamic analysis of a horizontally layered soil, Lysmer and Waas (1972). More recently this has been applied to a variety of static and dynamic problems Booker and Small (1979), however, for most analyses of deep underground openings it is usual to adopt an extensive finite element mesh.

In this paper the above difficulties are overcome by the development of the circular boundary element shown in Fig.1. The stiffness of this "super element" can easily by incorporated into a finite element analysis and used to analyse problems of the type illustrated in Fig.2 involving complex geometries and material problems.

It is interesting to note that an element similar to the one developed in this paper may be constructed from the well known analytic solutions to the problem of a circular hole in an infinite elastic body (Mushkhelishvili (1963)), however there are difficulties associated with both the number of terms necessary to obtain an adequate Fourier series representation and the conformity of elements based, on such an approximation, and conventional elements, and for these reasons the approach adopted in this paper was preferred.

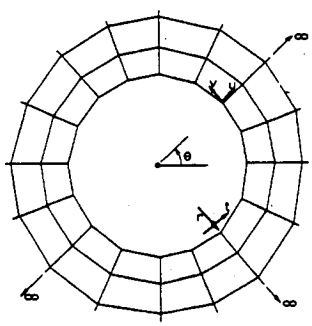

Fig. 1 Infinite Element

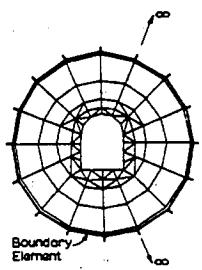

Fig. 2 Finite Element Mesh Incorporating Infinite Element

PROBLEM DEFINITION

Consider an underground opening, perhaps of the type illustrated in Fig.2. It will be assumed that the opening is sufficiently deep that the boundaries can be considered infinitely remote.

It will also be assumed that the underground opening is sufficiently long that conditions of plane strain prevail. Also it will be assumed that to sufficient accuracy the material responds elastically and that there are no significant changes in geometry so that small strain theory is valid.

Suppose then that the elastic continuum is divided into two portions as indicated in Fig.2. The inner portion is divided up into finite elements and the stiffness found using conventional theory, Zienkiewicz (1971), the outer region is broken up into quadrilateral elements, as shown in Fig.1. The theory is not restricted to the case of 4 node quadrilateral elements and can, for example, be easily extended to 8 node isoparametric elements.

The set of N circumferential nodes are assumed to be evenly spaced around the circular boundary. It proves convenient to develop the stiffness in terms of the radial and circumferential displacements (u_i and v_i) - see Fig.1. The elements in the inner region are linked to the elastic continuum through these nodes by the conditions of force equilibrium and displacement compatibility.

The element exhibits a polar periodicity which can be used to simplify the problem solution. In a closed form analysis of this problem the continuous displacement functions can be represented as a Fourier series in the angle θ. It is possible to employ a similar representation for the discrete case. Consideration of Fig.1 shows that each of the quantities (u, v, r, s) has a period of N, viz:

$$(\underset{\sim}{\delta},\ \underset{\sim}{f})_{k+N} = (\underset{\sim}{\delta},\ \underset{\sim}{f})_k$$

where $\underset{\sim}{\delta} = (u,\ v)^T$ and $\underset{\sim}{f} = (r,\ t)^T$

These functions may therefore be represented as a discrete Fourier series in the form:

$$(\underset{\sim}{\delta},\ \underset{\sim}{f})_k = \frac{1}{\sqrt{N}} \sum_{\ell=1}^{N} (\underset{\sim}{\Delta},\ \underset{\sim}{F})_\ell \exp(+\,i\alpha k\ell) \qquad (1)$$

where $\underset{\sim}{\Delta} = (U,V)^T$, $\underset{\sim}{F} = (R,T)^T$ and $\alpha = 2\pi/N$

and the Fourier coefficients are given by:

$$(\underset{\sim}{\Delta},\ \underset{\sim}{F})_\ell = \frac{1}{N} \sum_{k=1}^{N} (\underset{\sim}{\delta},\ \underset{\sim}{f})_k \exp(-i\alpha k\ell) \qquad (2)$$

It will be shown in the following sections that the introduction of the discrete Fourier representation leads to an upcoupling of the various modes so that the stiffness associated with each mode may be found separately.

DEVELOPMENT OF STIFFNESS MATRIX FOR A POLYGONAL RING

In order to develop the stiffness of the infinite element we first need to calculate the stiffness of the annular region shown in Fig.3. This ring is made up of N identical elements of the type shown in Fig.4 each having a stiffness matrix of the form:

$$\begin{bmatrix} \underset{\sim}{r}_k \\ \underset{\sim}{r}_\ell \\ \underset{\sim}{t}_k \\ \underset{\sim}{t}_\ell \end{bmatrix} = \begin{bmatrix} A & C & J & -K \\ C^T & A & K & -J \\ J^T & K^T & B & D \\ -K^T & -J^T & D^T & B \end{bmatrix} \begin{bmatrix} \underset{\sim}{u}_k \\ \underset{\sim}{u}_\ell \\ \underset{\sim}{v}_k \\ \underset{\sim}{v}_\ell \end{bmatrix} \qquad (3)$$

where A, C, B, D are symmetric matrices,

$\underset{\sim}{u}_{k,\ell}$ are the vectors of radial displacements for the sides k, ℓ respectively

$\underset{\sim}{v}_{k,\ell}$ are the vectors of tangential displacements on the sides k, ℓ respectively

$\underset{\sim}{r}_{k,\ell}$ are the vectors of radial nodel force for the sides k, ℓ respectively (due to the element kℓ)

$\underset{\sim}{t}_{k,\ell}$ are the vectors of tangential nodal force for the sides k, ℓ respectively (due to the element kℓ)

and $k = \ell + 1$.

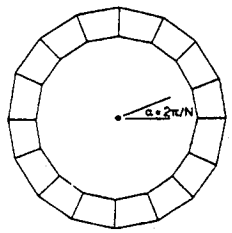

Fig. 3 Polygonal Ring Composed of Quadrilateral Elements

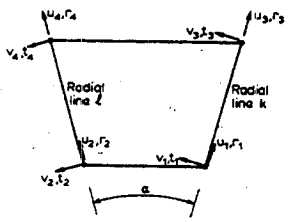

Fig. 4 Component Quadrilateral Element

The nodal forces acting at the nodes of a particular line consist of contributions from the two adjacent elements and thus, using Eq. (3), it is found:

$$\begin{aligned} &C(\underset{\sim}{u}_{\ell-1} + \underset{\sim}{u}_{\ell+1}) + 2A\,\underset{\sim}{u}_\ell - K(\underset{\sim}{v}_{\ell+1} - \underset{\sim}{v}_{\ell-1}) = \hat{\underset{\sim}{r}}_\ell \\ &-K^T(\underset{\sim}{u}_{\ell-1} - \underset{\sim}{u}_{\ell+1}) + 2B\,\underset{\sim}{v}_\ell + D(\underset{\sim}{v}_{\ell+1} + \underset{\sim}{v}_{\ell-1}) = \hat{\underset{\sim}{t}}_\ell \end{aligned} \qquad (4)$$

where the circumflex indicates the applied nodal force. Now on introduction of the Fourier representation, (3) these relationships become:

$$\begin{aligned} &[2A + 2cC]\,\underset{\sim}{U}_j + [-2iKs]\,\underset{\sim}{V}_j = \underset{\sim}{R}_j \\ &[+2iK^Ts]\,\underset{\sim}{U}_j + [2B + 2cD]\,\underset{\sim}{V}_j = \underset{\sim}{T}_j \end{aligned} \qquad (5)$$

where $c = \cos(\alpha j)$, $s = \sin(\alpha j)$

and the stiffness equations (4) separate into N sets of two equations, each with two unknowns. The analysis is faciliated by the change of variable

$$i\,\underset{\sim}{V}_j = \underset{\sim}{W}_j, \quad i\,\underset{\sim}{T}_j = \underset{\sim}{S}_j \tag{6}$$

and equation (5) becomes:

$$\begin{bmatrix} 2A + 2cC, & -2Ks \\ +2\,K^T s, & 2B + 2cD \end{bmatrix} \begin{bmatrix} \underset{\sim}{U}_j \\ \underset{\sim}{W}_j \end{bmatrix} = \begin{bmatrix} \underset{\sim}{R}_j \\ \underset{\sim}{S}_j \end{bmatrix} \tag{7}$$

For our purposes it is convenient to reorder the elements of the displacement and nodal force vectors using the permutation matrix P defined by:

$$\left[\underset{\sim}{D}^T_{jm},\ \underset{\sim}{D}^T_{jm+1}\right] = \left[\underset{\sim}{U}^T_{jm},\ \underset{\sim}{U}^T_{jm+1},\ \underset{\sim}{W}^T_{jm},\ \underset{\sim}{W}^T_{jm+1}\right] P^T \tag{8}$$

where $\underset{\sim}{D}_{jm}$ is $(U_{jm}, W_{jm})^T$ the vector of Fourier coefficients for the node polygon m with a similar definition for $\underset{\sim}{D}_{jm+1}$.

Equation (7) then becomes

$$\begin{bmatrix} \underset{\sim}{\Phi}_{jm} \\ \underset{\sim}{\Phi}_{jm+1} \end{bmatrix} = \begin{bmatrix} \Phi_j & \Psi_j \\ \Psi_j & \chi_j \end{bmatrix} \begin{bmatrix} \underset{\sim}{D}_{jm} \\ \underset{\sim}{D}_{jm+1} \end{bmatrix} = \kappa_j \begin{bmatrix} \underset{\sim}{D}_{jm} \\ \underset{\sim}{D}_{jm+1} \end{bmatrix} \tag{9}$$

where $\underset{\sim}{\Phi}^T_{jm} = (R_{jm}, S_{jm})$

and $$\kappa_j = P^T \begin{bmatrix} 2A + 2cC & 2Ks \\ -2K^T s & 2B + 2cD \end{bmatrix} P$$

DEVELOPMENT OF GENERAL BOUNDARY STIFFNESS

Suppose now that the consecutive rings making up the infinite element are chosen so as to have the same aspect ratio (i.e., same ratio of inner to outer radius) then it is well known that they will have identical stiffnesses. At any interior node there is no applied nodal force and so equation (10) leads to the recurrence relation:

$$\Psi^T_j \underset{\sim}{D}_{jm-1} + (\chi_j + \Phi_j)\,\underset{\sim}{D}_{jm} + \Psi_j \underset{\sim}{D}_{jm+1} = 0 \tag{10}$$

This recurrence relation has solutions having the form:

$$\underset{\sim}{D}_{jm} = \lambda^m \underset{\sim}{\Lambda} \tag{11}$$

where λ, $\underset{\sim}{\Lambda}$ satisfy the equation:

$$\left[\lambda^{-1}\Psi^T_j + (\chi_j + \Phi_j) + \lambda\Psi_j\right]\underset{\sim}{\Lambda} = 0 \tag{12}$$

this of course implies λ must satisfy the equation

$$\det\left[\lambda\,\Psi_j + (\chi_j + \Phi_j) + \lambda^{-1}\Psi^T_j\right] = 0 \tag{13}$$

If this determinant is expanded, it is found that, the resulting equation may be arranged as a quadratic in $(\lambda + 1/\lambda)$, and consequently, that equation (13) in general has four roots which may be written

$$\lambda_i = \{\lambda_1, \lambda_2, \lambda_3, \lambda_4\} \tag{14}$$

with $(\lambda_3, \lambda_4) = (\lambda_1^{-1}, \lambda_2^{-1})$ and $|\lambda| < 1$.

Now if the vectors $\underset{\sim}{\Lambda}_i$ are defined to be non-trivial solutions of the equation:

$$\left[\lambda_i^{-1}\,\Psi^T_j + (\chi_j + \Phi_j) + \lambda_i\,\Psi_j\right]\underset{\sim}{\Lambda}_i = 0 \tag{15}$$

the complete solution of the recurrence relation (10) may be written

$$\underset{\sim}{D}_{jm} = \sum_{i=1}^{4} A_i\,\lambda_i^m\,\underset{\sim}{\Lambda}_i \tag{16}$$

where $A_1, \ldots, A_4$ are arbitrary constants.

It is clear that in order that the solution may remain bounded at points remote from the hole, viz. as $m \to \infty$, the coefficients A_3, A_4 must vanish. The remaining coefficients may then be found as follows:

For the innermost ring equation (16) becomes:

$$\underset{\sim}{D}_{j_0} = \Omega \underset{\sim}{A} \tag{17a}$$

where $\Omega = [\underset{\sim}{\Lambda}_1, \underset{\sim}{\Lambda}_2]$ and $A^T = (A_1, A_2)$ (17b)

The Fourier coefficients of the nodal forces acting on the inner most ring are

$$\underset{\sim}{Q}_{j_0} = \Phi_j \underset{\sim}{D}_{j_0} + \Psi_j \underset{\sim}{D}_{j_1} \tag{18}$$

and thus we obtain the boundary stiffness

$$\underset{\sim}{Q}_{j_0} = k_{j_0} \underset{\sim}{D}_{j_0} \tag{19}$$

where

$$k_{j_0} = \Phi_j + \Psi_j \Omega^{-1} \begin{bmatrix} \lambda_1 & 0 \\ 0 & \lambda_2 \end{bmatrix} \Omega. \tag{20}$$

It is not difficult to establish that the boundary stiffness matrix is real symmetric and positive definite.

APPLICATIONS

The theory developed in the previous sections will now be illustrated by application the the behaviour of lined and unlined circular and elliptical openings in an elastic material. The effects of hydrostatic and non-hydrostatic field stress will be investigated.

Errors Involved In A Conventional Analysis

To illustrate the errors involved in a conventional analysis consider a circular tunnel of radius a opened in an elastic material which is initially in a state of hydrostatic stress.

$\sigma_{xx} = \sigma_{yy} = p$. As in well known the deflections and the changes in stress may be calculated by removing the radial traction p acting on the boundary r = a. Suppose now that in a conventional finitê element analysis the body is discretised by dividing the elastic body up into a number of rings with constant aspect ratio (ratio of inner to outer radius) and dividing each annulus into n four noded isoparametric elements with an aspect ratio of approximately unity, and assuming that a rigidly fixed outer boundary exists at r = b. The results of such an analysis are shown in Fig.5 where the percentage error in the tunnel deflection is plotted as a function of the position of the assumed outer boundary. The analytic solution and the solutions to the problem with b = ∞ using the boundary element are also shown in this figure and it may be observed that the conventional numerical solution to the problem is quite sensitive to the assumed position of the outer boundary. Thus if an outer boundary is taken at b/a = 5 the error in all conventional analysis is of the order of 12% whereas if a boundary element based on a division of each annulus into 20 elements is placed at the inner boundary the resulting solution is only 1% in error. Thus the use boundary elements has the advantage of leading to a considerable gain in accuracy as well as the more obvious effect of considerably reducing the number of equations to be solved and thus reducing computational and storage costs

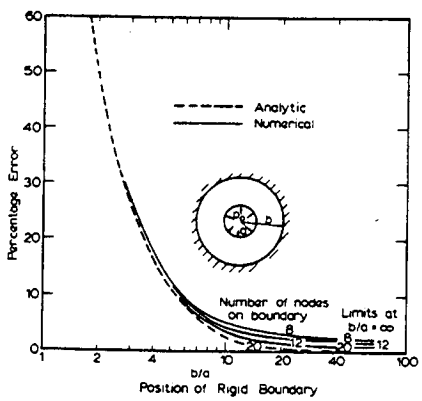

Fig.5 Effects of Finite Radial Boundary on Radial Displacement

Circular Cavity with Non-hydrostatic Loading

A problem of some importance to geotechnical engineers concerns the stresses and displacements which result when a deep tunnel is driven through a soil or rock deposit with a pre-existing non-hydrostatic field stress. Kirsch (1898) determined the stress distribution around a circular hole within a flat plate subjected to a uniaxial state of stress. This solution has been extended, with suitable adjustments to elastic parameters, to provide the stresses and displacements occuring in the vicinity of a deep tunnel, Terzaghi and Richart (1952).

Consider the elastic region between an internal circular cavity of radius a, and an external boundary of radius 10a. The external boundary is treated as being fixed, or as the internal boundary of the circular boundary element, with the intermediate region subdivided into an eight noded isoparametric finite element mesh. The numerical analysis was carried out under conditions of field stress $p_H = 1, p_v = 0$ with a number of different finite element discretisations and the two outer boundary conditions. The tunnel boundary conditions, those of zero normal and shear stress, are obtained from the initial stress state by applying appropriate stress increments i.e., normal and tangential tractions at the tunnel surface,

$$\sigma_n = -[p_H\cos^2\theta + p_v\sin^2\theta], \quad \tau = (p_H - p_v)\cos\theta\sin\theta$$

The stress increments obtained from the analysis are added to the initial field stresses to give the resulting stress state around the cavity. Through the use of superposition, the cavity response under any field stress conditions can be obtained from this analysis. The numerical solutions for displacement and stress are shown in Figs.6 to 8, and these satisfactorily approximate the analytical solutions which are shown in each of the figures. The effects of mesh design and external boundary condition on the displacement fields are also illustrated. The cavity response could, of course, be obtained through the use of the circular boundary element directly at the internal boundary.

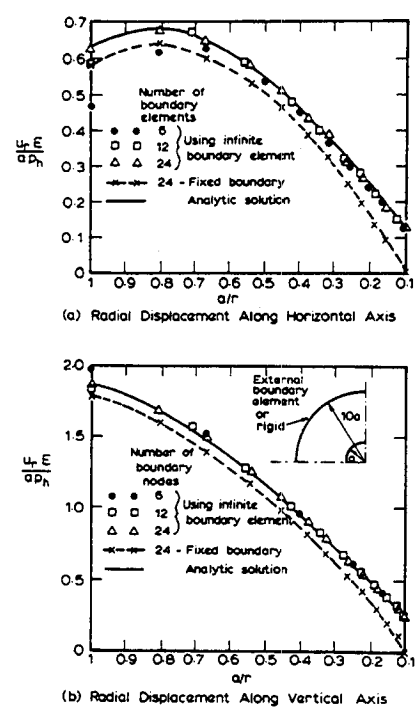

Fig.6 Behaviour of Circular Cavity under Field Stress

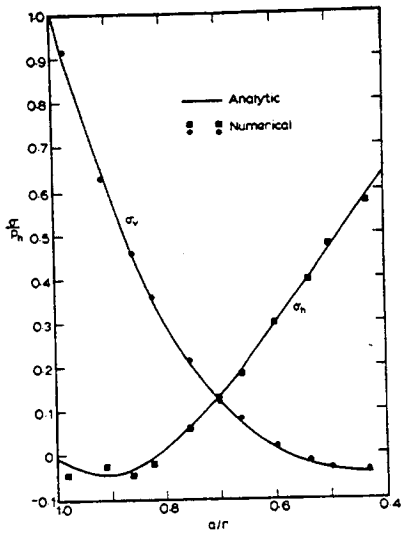

Fig.7 Horizontal and Vertical Stress on the Horizontal Axis

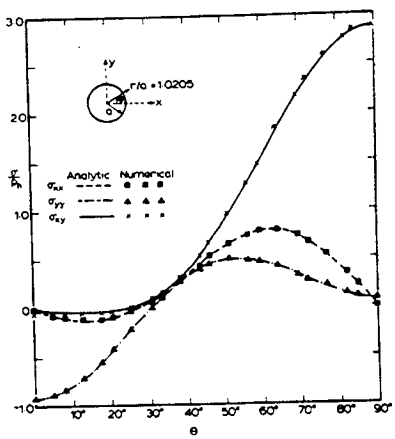

Fig.8 Stress Distribution Around the Circumference of an Opening

Elliptical Tunnel

Non-circular openings can also be analysed numerically using the boundary element, and the analysis can be extended far beyond those problems which have tractable analytic solutions. In order to demonstrate the analysis of non-circular cavities, one with an attendant analytic solution is now considered.

Neuber (1937) developed the solution equivalent to Kirsch (1898) for an elliptical hole. Terzaghi and Richart (1952) give details of Neuber's solution. In the numerical analysis the elliptical tunnel is modelled using an elastic region with an elliptical internal cavity and a circular external boundary, Fig.9. The field stresses used are again $p_H = 1$ $p_V = 0$ and are applied in the same was as those for the circular tunnel.

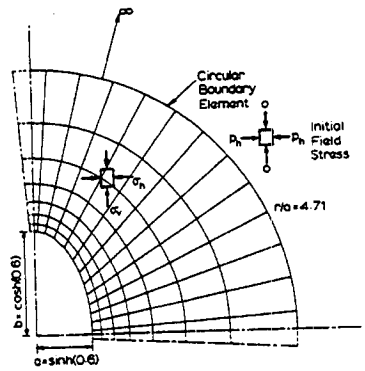

Fig.9 Mesh for the Determination of Stresses About on Elliptical Cavitv in an Infinite Continuum

The vertical stresses on the horizontal and vertical axes are plotted in Figs.10 and 11. The external boundary is again considered under two conditions - fully fixed and as the internal boundary of the circular boundary element. Figs.10 and 11 attest to the efficiency and accuracy of the numerical solution using the boundary element. The stress fields are fairly accurately modelled even where the stress gradients are severe, as they are on the vertical axis at the tunnel surface, Fig.11. The effects of a fixed external boundary on the stresses, at this distance are again quite severe - as is shown in the figures. The effect is obviously significant, and the external boundary would need to be repositioned further from the cavity, with a subsequent increase in the size and cost of the analysis.

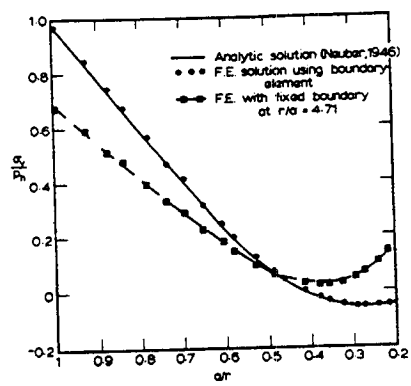

Fig.10 Vertical Stress on Horizontal Axis for an Elliptical Cavity

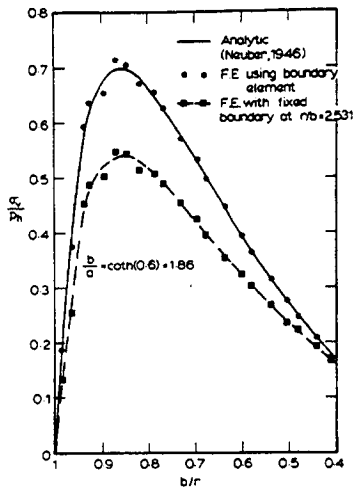

Fig. 11 Vertical Stress on Vertical Axis for an Elliptical Cavity

Lined Tunnels

When tunnelling in weak soil and rock deposits it is generally necessary to line the tunnel as it is constructed. A number of authors have investigated the elastic response of lined circular cavities, Hoeg (1968) and Muir-Wood (1975).

The problem considered consists of the construction of a circular cavity radius a, in an infinite elastic space with pre-existing non-hydrostatic field stresses. The lining, with elastic properties E_ℓ; ν_ℓ and thickness t is assumed to fully adhere to the elastic mass. Construction of the tunnel lining is assumed to take place prior to the removal of stress from the cavity surface, and thus boundary tractions identical to those used previously are applied to the internal boundary of the lining. A solution to this problem has been found using the classical theory of elasticity,* and compared with the corresponding numerical solution. For the particular case of co-efficient of lateral pressure K_o = 0.35, thickness to ratio t/a = 0.042, ratio of elastic moduli E_ℓ/E = 1720 and Poisson's ratios $\nu_\ell = \nu$ = 0.35. Stresses along the horizontal and vertical axes are shown in Figs.12 and 13. Radial displacements along the axes are given in Fig.14. The numerical results again agree closely to the analytic solution.

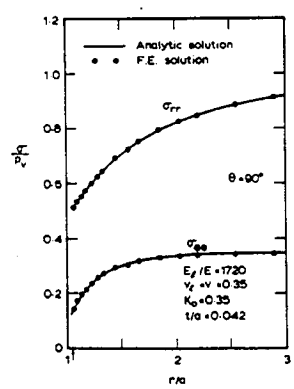

Fig.12 Radial and Tangential Stress for Lined Tunnel

*It was not possible to obtain a comparison with Heog"s (1968) solution which appears to be in error.

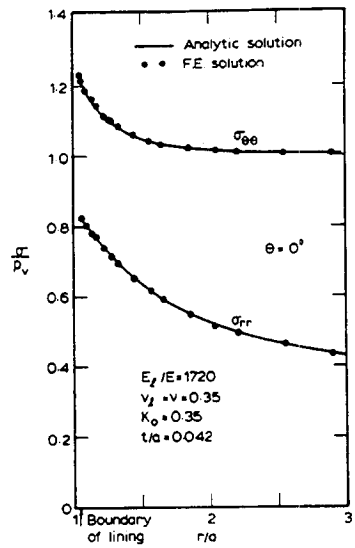

Fig.13 Radial and Tangential Stress for Lined Tunnel

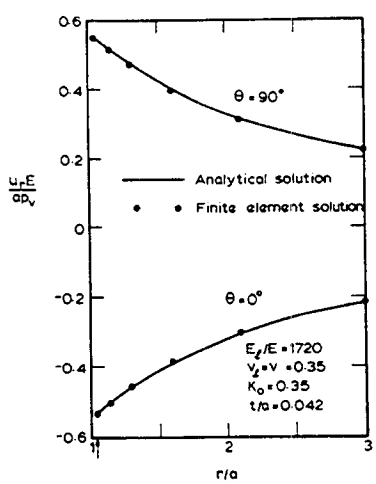

Fig. 14 Radial Displacement for Lined Tunnel

Lined Elliptical Tunnel

The circular boundary element can of course be used to examine problems not easily treated analytically. Such a problem is that of a lined elliptical cavity. The elliptical tunnel considered has similar geometry to the one already investigated, with horizontal axis a sinh (0.6) and vertical axis a cosh (0.6). Pre-existing field stresses considered are σ_V and $\sigma_H = K_o \sigma_V$, with three values for K_o - 0.5, 1.0 and 2.0.

The lining used has constant thickness t/a = 0.03, modular ratio E_ℓ/E = 1000 and Poisson's ratio $\nu_\ell = \nu = 0.25$. In the analysis the boundary element is used at a distance r/a = 1.6.

To illustrate the effects of lining the tunnel, Figures 15,16 show the contours of major and minor principal stress σ_1/σ_V and σ_3/σ_V in the soil surrounding the cavity. The stress states in the lined and unlined cases are shown, for

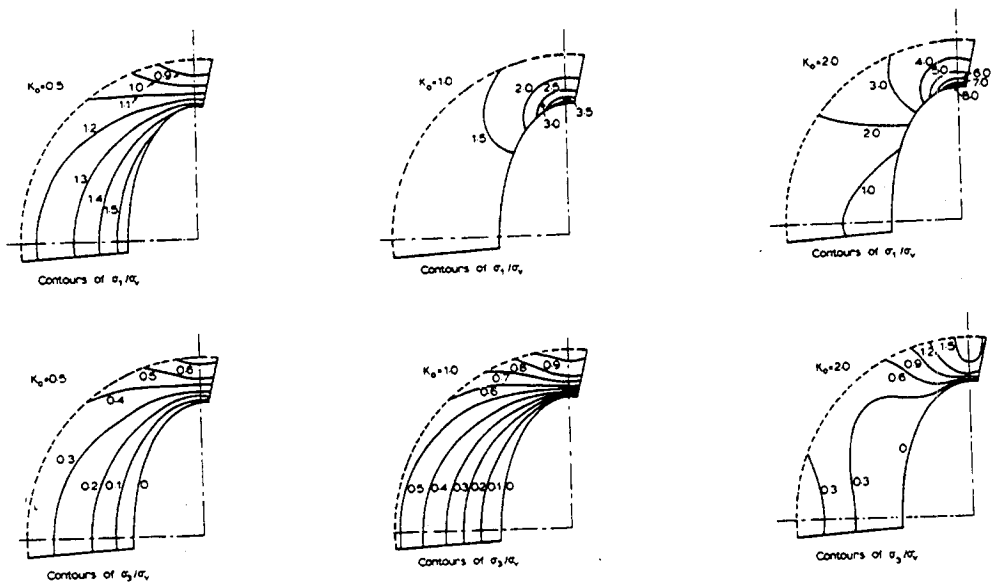

Fig. 15 Contours of Principal Stress for Unlined Tunnel

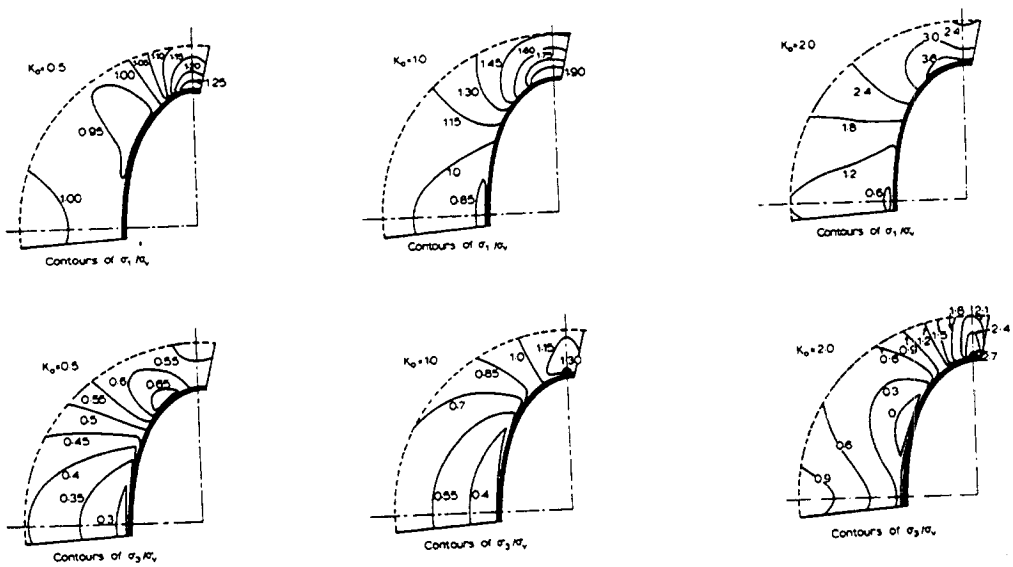

Fig. 16 Contours of Principal Stress for Lined Tunnel

the three values of K_o chosen. For the unlined cavity significant concentration of stress occurs around the opening - particular for the cases K_o = 1.0 and 2.0 where the high horizontal field stress is concentrated at the crown, the location of highest radius of curvature in the opening. The use of a lining significantly reduces the stress concentration which occur. This stress redistribution also results in some tensions developing close to the lining for the case where K_o = 2.0.

Due to the lining shape there is a change of sign of the resultant moment in the lining, shown in Figure 17b. A peak negative moment (clockwise) occurs at the crown of the tunnel, and this drops quickly, changing sign with the major portion of the lining experiencing an approximately uniform positive (anticlockwise) moment. A compressive axial load, Figure 17a, (likely to cause instability) is also induced in the lining, this is fairly uniform for the K_o - 0.5 and 1.0 cases, but peaks at the crown for the K_o = 2.0 case.

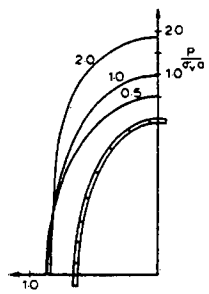

Fig. 17a Axial Force in the Lining-lined Elliptical Cavity

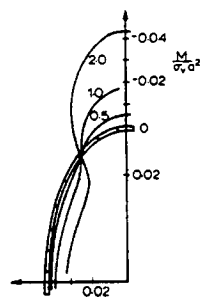

Fig. 17b Moment in the Lining-lined Elliptical Cavity

This straightforward elastic analysis illustrates many of the features of this type of structure, and the numerical procedure could, of course, be extended to model the effects of soil strength, the destablising effects of axial load on the lining stiffness and other features of soil-structure interaction.

CONCLUSIONS

A boundary element has been developed useful in the finite element analysis of deep underground openings. The circular boundary element facilitates efficient, economic and accurate modelling of a wide variety of problems. Its use is illustrated by the analysis of lined and unlined circular and elliptical tunnels. The method can be used for the analysis of inelastic behaviour and more complex cavity geometries. In a subsequent paper the development is extended to include more sophisticated elements, and problems of soil failure around tunnels and lining stability (buckling) will also be discussed.

REFERENCES

Booker, J.R. and Small, J.C., 1979. Finite Element Analysis of Problems with Infinitely Distant Boundaries. The University of Sydney, School of Civil Engineering, Research Report No. R356.

Hoëg, K., 1968. Stresses Against Underground Structural Cylinders. Jnl. Soil Mechs. Fndns. Divn., ASCE, Vol.94, No.SM4, pp.883-858.

Kirsch, G., 1898. V.D.I. Vol.42, 1898.

Lysmer, J. and Waas, G., 1972. Shear Waves in Plane Infinite Structures. Jnl. Eng. Mechs. Divn., ASCE, Vol.95, No.EM4, Proc. Paper 8716, pp.85-105.

Melan, E., 1932. Der Spannungszustand der durch eine Einzelkraft im Innern beanspruchten Halbschiebe, Z. Angew, Math Mech., Vol.12.

Muir-Wood, A.M., 1975. The Circular Tunnel in Elastic Ground. Geot. Vol.25, pp.115-127.

Mushkhelishvili, N.I., 1967. Rock Mechanics and the Mathematical Theory of Elasticity. P. Noordhoff Ltd., Croningen, Netherlands.

Neuber, H., 1937. Kerbspannungslehre. J. Springer, Berlin.

Obert, L. and Duval, W.I., 1967. Rock Mechanics and the Design of Structures in Rock. John Wiley and Sons, New York.

Savin, G.N., 1961. Stress Concentration around Holes. Pergamon Press.

Terzaghi, K. and Richart, F.E., 1952. Stresses in Rock around Cavities. Geot. Vol.3, pp.57-90.

Zienkiewicz, O.C., 1977. The Finite Element Method. McGraw-Hill, U.K.